CERN - European Organization for Nuclear Research

LCD-Note-2011-004

Development of the PANDORAPFANEW muon reconstruction algorithm

E. van der Kraaij*, J. Marshall†

* *CERN, Switzerland*

† *University of Cambridge, Cavendish Laboratory, Cambridge CB30HE, UK*

June 1, 2011

Abstract

The development of the current muon reconstruction in the PANDORAPFANEW particle flow algorithm is presented. First, an introduction to PANDORAPFANEW and a comparision of the signals from muons and pions in the calorimeter is presented. Then, the muon reconstruction algorithm is introduced. Finally, the performance is tested on both isolated muons and muons in high multiplicity events, and found to be adequate. Background signals from beam halo muons are also discussed and possibilities of reconstructing them are suggested.

Contents

1 Introduction

The detectors concepts at the linear colliders ILC and CLIC are designed with the particle flow approach in mind. Particle flow algorithms aim to reconstruct the four-vectors of all detected particles in an event. This note describes the muon reconstruction algorithm implemented in PANDORAPFANEW. The current study is performed for the CLIC detectors, yet the algorithm could be used in ILC detectors as well.

After an introduction to PANDORAPFANEW and the tools used in this analysis, we discuss some basic properties of muons and hadrons reconstructed as Particle Flow Objects (PFOs) in Section 2. Pions are considered, as their signals in the detector can resemble those of muons: First, before a pion showers, it is a minimum ionizing particle, just like a muon. Second, a pion can decay in flight creating a muon.[1)] Finally, a pion can punch through to the muon system. The hits it deposits there can mistakenly be interpreted as a muon signal.

In Section 3 we go through the new muon reconstruction algorithm step by step. The performance of the algorithm is presented in Section 4. In Section 5 we discuss an outstanding issue: beam halo muons. Created in the accelerator complex and traversing the detector approximately parallel to the beam lines, their high flux may pose a serious problem in the reconstruction of events.

1.1 PANDORAPFANEW

PANDORAPFANEW is a framework for developing and running particle flow algorithms. It currently offers more than 60 high performance and well-documented algorithms for particle flow reconstruction and particle identification in fine granularity detectors [1]. The Particle Flow reconstruction Algorithms (PFA) aim to reconstruct the four-vectors of all detected particles in an event. Jets can subsequently be reconstructed by jet-clustering algorithms, with the reconstructed jet energy being the sum of the energies of the individual PFOs.

In a particle flow reconstruction, the momenta of charged particles are measured in the tracking detectors, whilst only the energy measurements for photons and neutral hadrons are obtained from the calorimeters. The hadronic calorimeter is thus used to measure about 10% of the energy in a jet, resulting in significantly better resolutions than those obtained from conventional calorimetry.

However, double counting of energy depositions can occur when depositions in the calorimeter are not assigned to the correct reconstructed particle. This *confusion*, rather than classical calorimetric performance, is the limiting factor in particle flow calorimetry. Sophisticated software algorithms are therefore required, alongside fine granularity calorimeters, which help to reduce the confusion.

In summary, the PANDORAPFANEW particle flow algorithms perform the following operations to build a PFO:

1. Calorimeter hits (from the ECAL and HCAL) and tracks in the event are examined and objects are created for use in the subsequent reconstruction. Calibration factors are applied

[1] The probability is less than 1% for a pion with 10 GeV or more.

to hit depositions. Quality cuts are used to select suitable tracks, which are then used for PFO construction.

2. Hits are clustered using a cone-based outward projective algorithm, working from innermost to outermost layer. Isolated hits in the calorimeters (defined on the basis of proximity to other hits) are neglected in this initial clustering.

3. The clustering algorithm is configured so that it tends to split up true clusters, rather than risking combining energy deposits from multiple particles. The resulting cluster fragments are then merged together in a series of algorithms following well-motivated topological rules. Isolated hits are added back into the collection at this stage.

4. Calorimeter clusters are associated to tracks, by comparing the properties of the clusters and the projected track states at the surface of the calorimeter.

5. If the energy of a calorimeter cluster does not match the associated track momentum, the cluster can be split-up, or merged with nearby fragments, by a number of statistical reclustering algorithms. The calorimeter hits in the relevant clusters can be reclustered using a series of differently configured clustering algorithms to try to improve the track-cluster compatibility.

6. Fragments of charged hadrons are identified and removed, then the final PFOs are constructed. If a PFO contains tracks and associated clusters, the particle properties are extracted from the tracks. For neutral particles, calorimeter information is used and plugin particle identification functions are used to label particle types and to distinguish between photons and neutral hadrons.

The above processes are described in more detail in [1, 2].

1.2 Detector design

CLIC_ILD_CDR is one of the two CLIC detector concepts. It is a general purpose detector designed with both the tracking sub-detectors and the calorimeters inside a superconducting solenoid. In the transverse plane through the interaction point, the electromagnetic and the hadronic calorimeter have a depth of 1 and 7.5 λ_I respectively. The solenoid is surrounded by an iron yoke. The yoke is composed of large iron slabs interleaved with active muon layers.

The hadronic calorimeter consists of 75 active layers in the barrel with readout cells of 30×30 mm^2. The muon system consists of nine and ten layers in the barrel and the endcaps respectively, with the same cellsizes as in the HCAL. The detector geometry in the simulation program is described in [3]. The muon detector system is described in more detail in [4].

1.3 Tools used

For all event samples listed in this section the full detector response of CLIC_ILD_CDR is simulated in MOKKA using GEANT4 [5]. The reconstruction is performed with ILCSOFT, using the MARLIN binary [6]. PANDORAPFANEW is available as part of ILCSOFT.

1.3.1 Performance monitoring

As a quality check, the performance of the muon identification is assessed. To this end, a reconstructed muon is defined as matched to a generated muon provided the angle between the momentum direction of the two is less than 1°, and provided the reconstructed transverse momentum $p_{\mathrm{T}}^{\mathrm{reco}}$ is less than 5% away from the generated muon p_T^{MC}.

The efficiency is defined as the number of matched muons divided by the number of generated muons. Only generated muons with energies above 7.5 GeV and with a polar angle $\theta > 8^\circ$ are considered. The purity is defined as the number of matched muons divided by the number of reconstructed muons. The algorithm used to monitor the performance is described in detail in [7].

1.3.2 Samples studied

Muon and pion particle gun: The detector response to single muons and pions is simulated by using the particle gun in MOKKA. For both particle types up to $4 \cdot 10^5$ events were created where the particle direction varied over the full range in polar and azimuthal angle. The energy of the particles varied between 5 and 1000 GeV.

Isolated muons in supersymmetry channel: The performance of the algorithm on highly energetic isolated muons is tested with a sample of 10^4 $e^+e^- \to \widetilde{\mu}_R\widetilde{\mu}_R$ events. These are generated according to the CDR smuon benchmark process [8]. The supersymmetry channel has smuon mass $m_{\widetilde{\mu}_R} = 1010.8$ GeV and the final state forms a clean environment with two isolated muons and missing energy.

Muons in high-multiplicity environments: For thorough testing of the muon reconstruction algorithm the full reconstruction of a sample of 9000 $e^+e^- \to Z^\star \to b\bar{b}$ events is used. These were generated with PYTHIA [9], with a center-of-mass energy of 1.5 TeV. Each event has at least one of the b-quarks decaying leptonically through a muon. With this sample the challenging task of reconstructing muons in dense highly-energetic jets at CLIC can be mimicked: at a center-of-mass energy of 1.5 TeV the sample of jets resembles the b-jets to be expected in 3 TeV collisions with a final state of four b-jets.

2 Muon and pion PFO properties

The reconstruction of single muons and pions by the PFA is studied using the particle gun samples. With these samples the PFOs that are created indicate how the algorithms perform without confusion from overlapping particles.

In Figure 1 a schematic view is depicted of typical muon and pion hits created in several calorimeter layers. A wide shower is created by the pion as it interacts with matter in the calorimeter. The muon leaves a trail of hits. It can scatter, but for high energies it is most often a straight line.

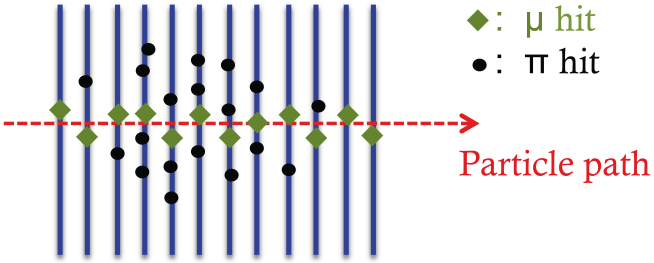

Figure 1: *Schematic view of hits deposited by muons and pions in the hadronic calorimeter.*

2.1 Shower shapes in the hadronic calorimeter

For each track and its associated cluster, the PFA will create a PFO. After creating a distribution of the absolute distances for each hit in one PFO to the PFO axis[2)], we can obtain an average distance and RMS per PFO.

Extracting the average distance and RMS of the hit distance distributions for muons and pions we obtain the results of Figure 2. Samples of 1000 particle gun events are used, with the muon or pion generated with exactly 100 GeV, freely varying in the azimuthal angle. In order to avoid varying the angle of particle impact on the readout layers, the polar angle is fixed to an angle of arbitrary choice in the barrel, $\theta = 73°$. The results in the figure are for the hits clustered in the hadronic calorimeter. We emphasize that at this point no muon reconstruction algorithm is applied. The hits in the muon system are not considered yet.

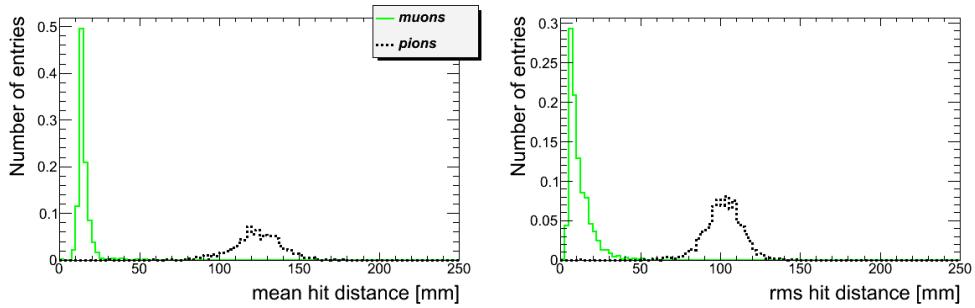

Figure 2: *For the clusters in the HCAL: the figure left shows the mean distances of the hits in muon and pion PFOs. The figure right shows the RMS of the hit distance distribution in muon and pion PFOs.*

These results show how the PFA reconstructs the particles. The muons, leaving only a fine trail of hits, have low mean distances with small RMS. The pions have much larger mean values and higher RMS, showing that the PFA can reconstruct wide shower shapes.

[2]Defined by the energy-weighted distribution of the hits.

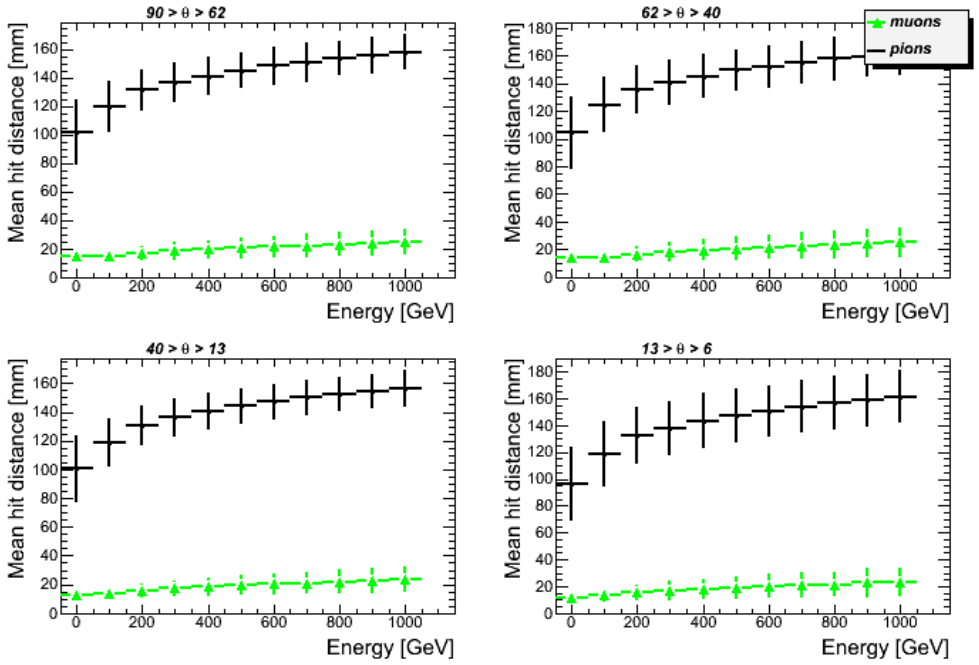

Figure 3: *Mean distance of all hits to the PFO axis in the HCAL versus the energy, calculated from muon and pion particle gun sample.*

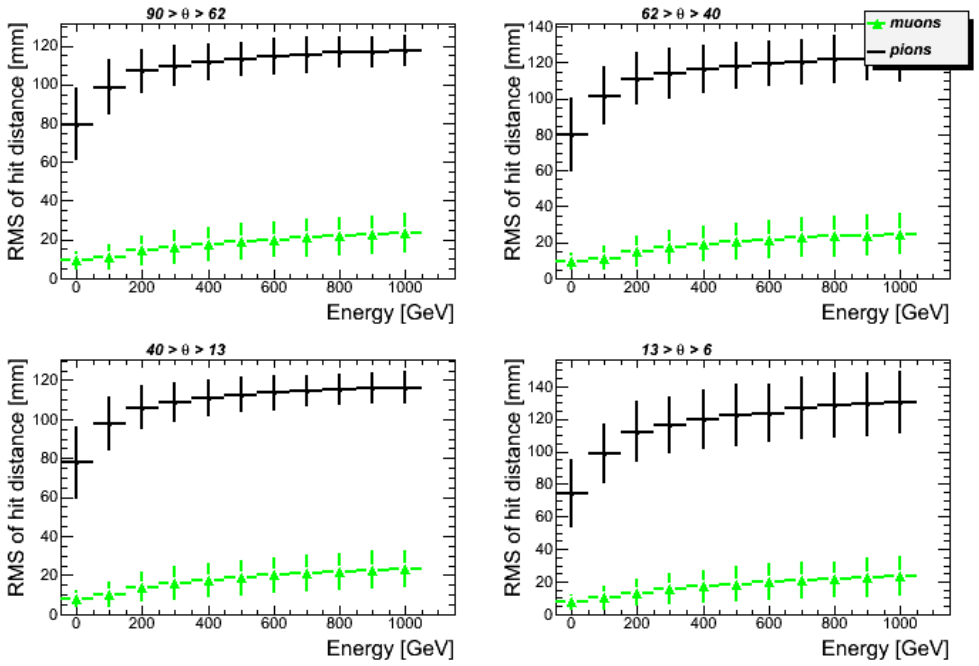

Figure 4: *RMS of the distances of all hits to the PFO axis in the HCAL versus the energy, calculated from muon and pion particle gun sample.*

Repeating the analysis for a larger range of energies produces the results shown in Figure 3 and 4. These show the mean distances and RMS of the hit distributions in the HCAL, as functions of the particle's energy. To see if the angle of impact on the calorimeter layer is of importance, the samples are divided in four regions of the polar angle: the barrel $(90° > \theta > 62°)$, the transition region from barrel to endcap $(62° > \theta > 40°)$, the endcap $(40° > \theta > 13°)$ and the very forward region $(13° > \theta > 6°)$. No significant difference is visible.

The statistical uncertainties on these results are negligible; the uncertainty bars in the figures are defined by the width of the distributions. In other words, the bars in Figure 3 are the widths of the distributions in the left figure of Figure 2, the bars in Figure 4 are the widths of the distributions in the right figure of Figure 2.

The figures show that for both muons and pions the showers increase in size with energy. However, the 'showers' created by the muons remain much smaller over the full energy range. In the hypothetical case of isolated muons and pions, the information from the hadronic calorimeter is therefore sufficient to distinguish the two particle types.

2.2 Shower shapes in the muon system

Pions can punch through the calorimeter into the muon system. In Figure 5 the fraction of pions that make it through to the muon system is shown as a function of the energy in the four previously mentioned regions. A pion is defined to punch through, provided it deposits a cluster

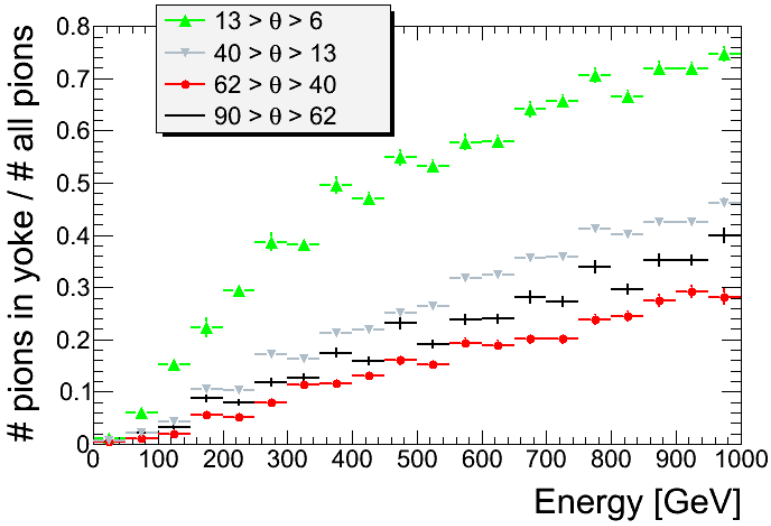

Figure 5: *Fraction of pions, shot with the particle gun, that punch through to the muon system as a function of the energy.*

of at least three hits in the muon system. A dependence on the polar angle can be seen, showing a clear reflection of the material distribution before the muon system, see [3].

Applying the same analysis from the previous section to the muon layers, large variations are seen. This is as expected and, in contrast to the situation in the HCAL, the shower shapes in the muon system cannot be used to distinguish muons from pions.

3 New muon reconstruction algorithm

The previous section illustrates that the cone-based outward projective clustering algorithm of PANDORAPFANEW works well for isolated muons and pions. However, for muons inside jets it turns out that in the HCAL the confusion, mentioned in Section 1.1, is too large; the relative small number of hits deposited by a muon, among the many hits produced by other particles in the jet, cannot always be reconstructed as belonging to each other.

With the information available, an inward projective muon reconstruction turns out to be more effective. The trail of hits deposited in the muon system can be identified and then matched to a track in the tracking sub-detector. Extrapolating the direction of the inner detector track to the track in the muon system, the muon hits deposited in the calorimeters can then be identified.

An important constraint for the muon reconstruction algorithm is that the final jet energy resolution is not degraded: By performing the muon reconstruction as the first step in the event reconstruction, muons can be removed from the event, potentially reducing the confusion encountered by the subsequent reconstruction algorithms. However, the muon reconstruction process could also cause problems, by wrongly identifying hits as originating from or a muon, or incorrectly removing a track from the tracking sub-detectors. Such problems would immediately deteriorate the jet energy resolution.

The muon reconstruction algorithm was developed in the PANDORAPFANEW framework. This framework provides a large number of tools to ease algorithm development. Many functions are provided to investigate cluster topologies, and the memory-management is made simple. We now consider the different steps of the new algorithm:

1. Identification of yoke track candidates.
2. Extrapolation of inner detector tracks to muon system.
3. Matching of inner detector tracks and yoke tracks.
4. Identification of hits deposited by the muon in the ECAL and HCAL.

3.1 Identification of yoke track candidates

To identify the tracks of muon hits in the muon system the same cone-based clustering algorithm as used in the hadronic calorimeter is applied, see also Section 1.1. However, the algorithm is configured so as to deal with the limited number of layers in the muon system. The following settings were found to address the vast majority of cases:

- `ShouldUseIsolatedHits` — In the yoke plug layer a muon can deposit a single hit. In order to include such hits in the clustering, this parameter is set to `TRUE`.
- `TanConeAngleCoarse` — The tangent of the angle of the cone used to search for new hits. This parameter is set to 0.3.

- `ConeApproachMaxSeparation` — The maximum distance between two hits to be allowed to be clustered together. The distance between muon layers is large and this parameter is set to 2000 mm.
- `MaxClusterDirProjection` — The maximum distance, projected on the cone axis direction, over which new hits are looked for. This parameter is also set to 2000 mm.
- `AdditionalPadWidthsCoarse` — In the clustering cone, the maximum distance a hit candidate can be from the cone's axis is defined by the `TanConeAngleCoarse`. As the location of a hit is defined by the center of a readout cell, a cell hit inside the clustering cone can still be regarded as too far. The maximum distance to the cone axis can therefore be increased with the parameter `AdditionalPadWidthsCoarse`. This parameter is set to 1, adding an additional distance of one cellsize.
- `SameLayerPadWidthsCoarse` — This parameter defines how far neighboring hits in the same muon layer may be separated. In order to only cluster immediate neighbors, this parameter is set to 1.8 (with one unit being the length of a readout cell).

Applying the clustering algorithm with the above settings to the b-jets sample, mentioned in Section 1.3.2, clusters in the muon system are obtained with the properties shown in Figure 6. We see that most muons form clusters of at least nine hits, covering eight or nine layers. Some clusters cover more than nine layers: these traverse the detector in the transition region from barrel to endcap. These properties are as expected from the detector geometry [4]. Clusters deposited by other particles cover on average fewer layers and contain on average fewer hits.

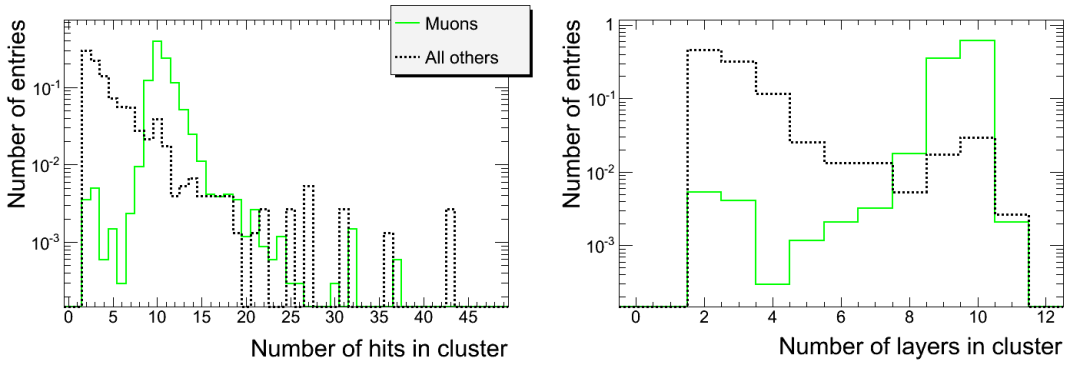

Figure 6: *Number of hits (left) and number of layers (right) in clusters reconstructed in the muon system. A cluster's particle type is obtained from the outermost hit: if deposited by a muon, the cluster is considered a muon cluster. If not, the cluster falls in the 'other' category. The cluster is to be deposited by a particle with an energy of more than 7.0 GeV and a polar angle of more than* 8°.

With these results we come to the following selection criteria: a cluster reconstructed in the muon system is considered as a muon yoke track if it occupies eight or more layers, yet contains

no more than 30 hits. Applying a cut on the maximum number of hits helps to avoid large punch-throughs from the calorimeter into the muon system. The user is free to change the two settings with the steering parameters `MinClusterOccupiedLayers` and `MaxClusterCaloHits` respectively. An additional parameter is the `MinClusterLayerSpan`: it defines the maximum 'depth' of a cluster, i.e. the difference between the last and the first layer number. The default value is also chosen to be eight.

3.2 Extrapolation of inner detector tracks to the muon system

For the extrapolation of the ID-track, the magnetic field strength must be known. Presently, the B-field map in the CLIC_ILD_CDR simulation is much simplified: 4 T inside the solenoid, -1.5 T in the muon barrel and 0 T in all other areas.

With the momentum and direction of an ID-track and the magnetic field a helix is created. At the intersection of the helix with the solenoid middle radius, or when the helix exits the solenoid towards the endcap, the helix direction is altered: an *external helix* is calculated taking into account the strength of the field outside the solenoid.

3.3 Matching of inner detector and yoke tracks

The next step is to find the ID-track matching to the yoke track. For each yoke track all ID-tracks are considered and two variables are calculated:

- **Distance of closest approach:** shortest distance of the external helix to the mean position of the hits in the innermost layer of the yoke track.
- **Directions angle:** angle between the direction of the external helix at its entry point to the muon system and the direction of the yoke track. The latter is obtained from a straight line fit to the distribution of hits in the yoke track. This fit accounts for any variations in the sizes of instrumented cells.

Considering only selected yoke tracks truly originating from muons (selected using MC information), we see in Figure 9 the correlation between the two variables. The distributions are shown separately for ID-tracks with less or more than 10 GeV; a cut to help distinguish tracks with appreciable bending from tracks with negligible bending.

The upper right plot of Figure 9, with the results for matched tracks[3)] of high energies, shows that most have opening angles of no more than 0.1 radians. The distances of closest approach are mostly below 100 mm. From the upper left figure, with the results for correctly matched tracks of low energies, we can see that both the angle and distance of closest approach reach larger values. This is expected: as the yoke track direction is obtained from only a straight line fit through the cluster, low energy muons are less accurately reconstructed.

The lower figures show that the non-matched tracks have larger angles and distances. With these four figures in mind it is decided to select the best ID-track candidate as the track with the smallest distance of closest approach. The track must have an energy of at least 7 GeV;

[3]The track is defined as matched when its "Monte Carlo unique PID", a unique code referring to the particle it originates from, is identical to the unique PID of the outermost hit of the yoke track.

a value that can be changed via the steering parameter `MinTrackCandidateEnergy`. Additional quality cuts are applied to disregard candidates with opening angles of more than 0.2 rad or distances of more than 200 mm. These values can be altered via the steering parameters `MinHelixClusterCosAngle`[4)] and `MaxDistanceToTrack`.

The default values for these two quality cuts are chosen from the results depicted in Figure 10. This figure shows the identification performance of the muon algorithm with different values for the quality cuts: the distance cut of 200 mm is chosen as to keep the purity as high as possible. In order to also obtain a satisfactory efficiency an angular cut of 0.2 rad is chosen.

3.4 Identification of muon hits in the calorimeter

With the previous steps the muon four-vector can already be constructed: the direction as well as the momentum can be determined from the ID-track. For an optimal jet reconstruction performance it is important to also identify the hits in the calorimeter originating from a muon. The steps for this hit identification are:

- For each pairing of muon ID-track and yoke track, the available non-isolated calorimeter hits in each layer are considered. These hits must have an expected direction in close agreement with the direction of the track helix, when extrapolated to the hit position. This agreement is controlled via the parameter `MinHelixCaloHitCosAngle`, which has a default value of 0.95.

- The generic distance between each hit and the track helix is defined as the ratio between the helix-hit distance and the 'length scale' of the calorimeter cell. This generic distance is calculated for each hit in a layer and the hits are ordered by increasing distance. At the same time, the number of hits within two regions (`Region1GenericDistance` < 3 and $3 <$ `Region2GenericDistance` < 6) are counted to assess whether the muon is isolated in the layer.

- Isolated muon layers are judged to be those with one or more hits in region 1, controlled via the parameter `IsolatedMinRegion1Hits`, and zero hits in region 2, controlled via `IsolatedMaxRegion2Hits`.

- Hits are added to the muon cluster in order of increasing distance. If the muon is not isolated, only the single closest hit in the layer is added, provided it is within six generic distances (`MaxGenericDistance`). If the muon is isolated, all hits in the layer within three generic distances are added (`IsolatedMaxGenericDistance`).

All layers between the inner tracking detectors and the muon yoke are considered. This process completes the identification of the components (calorimeter hits and tracks) in the muon PFO.

[4] An opening of 0.2 rad corresponds to the parameter `MinHelixClusterCosAngle` set to 0.98.

3.5 All steering parameters

In Table 1 all the steering parameters which have been mentioned in the previous sections, including the default values, are summarized. These parameter values can be altered by the user.

Steering parameter	Default value
TanConeAngleCoarse	0.3
ConeApproachMaxSeparation [mm]	2000.
MaxClusterDirProjection [mm]	2000.
ShouldUseIsolatedHits	True
AdditionalPadWidthsCoarse	1
SameLayerPadWidthsCoarse	1.8
MaxClusterCaloHits	30
MinClusterOccupiedLayers	8
MinClusterLayerSpan	8
MinHelixClusterCosAngle	0.98
MaxDistanceToTrack [mm]	200
MinTrackCandidateEnergy [GeV]	7.0
Region1GenericDistance	3
Region2GenericDistance	6
IsolatedMinRegion1Hits	1
IsolatedMaxRegion2Hits	0
MaxGenericDistance	6
IsolatedMaxGenericDistance	3

Table 1: *Steering parameters that can be altered by the user, and their default settings. The first six parameters steer the clustering of the hits in the muon system. The next three are to define the muon system cluster candidates. The next three select the inner detector tracks. The final six select the hits in the calorimeter.*

4 Reconstruction performance

To discuss the final performance of the muon reconstruction algorithm we show in Figure 11 the efficiency and purity obtained with the muons in high multiplicity b-jet events. For comparison the performance for isolated muons with similar energies is also shown; the latter are generated with the particle gun. In Figure 12 the performance is shown with the reconstruction algorithm applied to the supersymmetry sample with high energy muons.

For isolated muons with $\theta > 10^\circ$ and energies of more than 7.5 GeV efficiencies and purities of $> 99\%$ are obtained. For muons in high multiplicity events the lower limits are approximately 90%, except for the efficiency at $\theta \sim 60^\circ$: the large distance from the inner detector to the muon system influences the performance. From the efficiency results we also see that in the transition region from barrel to endcap, at $\theta \sim 40^\circ$, the performance is slightly worse.

5 Beam halo muons in the detector

In this section we discuss the possibility of identifying the hits deposited by beam halo muons in the detector. We use a sample of simulated beam halo muons generated by L. Deacon, similar to the sample used for the study described in [10]. The sample consists of $2.2 \cdot 10^5$ muons created in one beamline and is to be normalized to $2.4 \cdot 10^4$ to obtain the occupancy in the time interval of one train: in [11] it is concluded that the total number of beam halo muons entering the detector is $1.2 \cdot 10^4$. Considering that the detector is approached from both sides, this number has to be doubled to $2.4 \cdot 10^4$ to determine the final occupancy. This final number depends strongly on the type of spoilers used in the beamline. Therefore, a considerable reduction of the beam halo muons is certainly possible. More details on the occupancy and their consequences for the detector readout technologies are discussed in [4].

Figure 7 presents the energies and the detector entry points of the beam halo muons. Shown are the properties of the muons as they enter the detector; no detector response is simulated yet. The upper left shows the energy distribution of the beam halo muons. Approximately 25% have an energy of up to 25 GeV, yet the distribution is wide and in extreme cases, 1 TeV beam halo muons enter the detector.

In the upper right figure the radial distribution is shown, where the radius is the distance of the beam halo muon to the beam axis at the detector entry point. We see that almost all muons enter

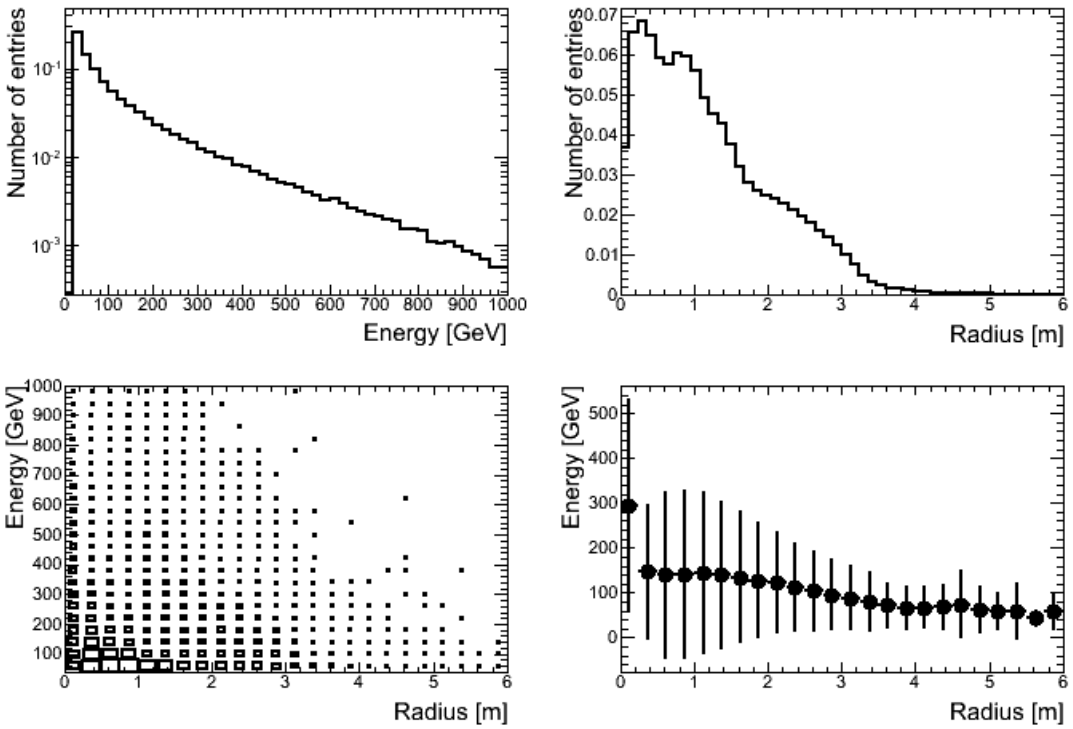

Figure 7: *The beam halo muon energies and detector entry points. See text for more detail.*

the detector within a radius of 3 m. Note that the momenta of all muons can be approximated as being parallel to the beam axis.

In the lower two figures the distribution of the energy versus the radius is depicted in two different ways, showing that the spread in energy is present over the full detector.

The total energy deposited by all beam halo muons in the detector is significant. To prevent clustering confusion, their hits will have to be identified before the clustering algorithm starts the reconstruction from the interaction point. For the PFA the muons passing horizontally through the calorimeter barrel are the biggest problem: as the deposited hits have no associated track pointing to the interaction point, the hits are interpreted as originating from neutral particles. Being numerous, this can have a significant impact on the jet reconstruction.

Reconstructing beam halo muons is, however, not an easy task, especially for the lower energies. Those traversing the calorimeter barrel will pass in total through ~ 14 m of material, among others tungsten and iron. Assuming a conservative average density of 7 g/cm^3 and a mean energy loss of 2 MeV per g/cm^2 for a muon, see [12], we find an average loss of 20 GeV for a muon traversing the entire detector. A substantial fraction of the beam halo muons will thus end up being absorbed in the detector.

High energy muons can quite easily be identified. On a sample of 1000 muons generated with 50 GeV with the MOKKA particle gun through the CLIC_ILD_CDR detector (at a radius of 2.5 m) we applied a few of the tools of the muon reconstruction algorithm:

- First, the same clustering algorithm as in Section 3.1 is applied to obtain the two yoke tracks in both endcaps. Out of 1000 muons, 887 have two good yoke tracks.
- Second, without considering the magnetic field, the yoke track in the endcap first hit by the particle gun, the 'first yoke track', is extrapolated to the other side of the detector.
- Finally the distance of closest approach to the innermost hit of the second yoke track is calculated, together with the opening angle between the two fitted yoke track directions. The results obtained are presented in Figure 8.

The distances and angles do not differ significantly from the muons considered in the previous sections. Applying similar techniques as in the regular muon reconstruction algorithm can thus be helpful in reconstructing beam halo muons with energies of at least 50 GeV.

It should be emphasized that the above results have been obtained on single muons generated with a particle gun. In [4] it is calculated that at the inner radius of the muon system endcap the occupancy per cell per ns is $\sim 3\%$. A cell is 30×30 mm^2; this implies that within 200 mm distance of a beam halo muon track a total of nearly five muons can be expected in a time window of 1 ns. It is unclear for the moment whether the resulting combinatorial problem can be resolved.

However, with many of the muons being absorbed in the detector, it is felt that efforts should first be concentrated on reconstructing low energy muons. In [4] it is concluded that multi-hit readout capability has to be foreseen in the muon system endcaps to handle the high occupancy. Combining multi-hit readout with the excellent time resolution of RPCs, which is better than 1 ns, offers the possibility to identify the direction of yoke tracks. Once an inward yoke track is thus identified, it can then be projected into the hadronic endcaps and, continuing inwards, much

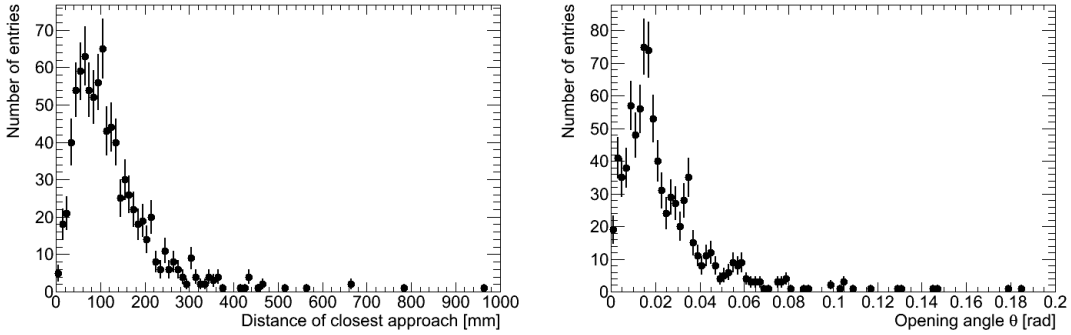

Figure 8: *Extrapolating one yoke track obtained from a beam halo muon to the yoke track in the second endcap, the distance of closest approach is obtained (left) and the opening angle (right).*

information can be gained on the path of the muon throughout the entire detector. Applying such algorithm to higher energy muons could then also be useful to better determine the entry point of the muon in the second endcap.

6 Summary

A new muon reconstruction algorithm has been developed in the PANDORAPFANEW framework. It has been tested in the CLIC_ILD_CDR concept, one of the two detectors studied in the CLIC conceptual design report.

The algorithm defines, as a first step, muon candidates by fitting straight tracks through hits clustered in the muon system. By extrapolating the inner detector tracks outwards and identifying the best matched track, the muon four momentum is reconstructed by the inner detectors. The algorithm performance is good: for isolated muons with $\theta > 10^{\circ}$ and energies of more than 7.5 GeV, efficiencies and purities of $> 99\%$ are obtained. For muons in high multiplicity events the lower limits are approximately 90%.

Two aspects of the algorithm will require attention in the future: first, the straight track fitting through the hits in the muon system results in worse performance for low energy muons. Second, with only a basic B-field implemented at the moment in the simulation the extrapolation of the inner detector track to the muon system is straightforward. Any change in B-field mapping would require the muon reconstruction algorithm to be re-evaluated.

The phenomenon of beam halo muons has briefly been discussed. High energy muons (more than 50 GeV) might easily be reconstructed. At lower energies a large fraction of the muons will, however, be entirely absorbed by the detector. Identifying their energy deposition is non trivial and requires further studies.

7 Acknowledgements

We would like to thank Jacopo Nardulli for providing the identification monitoring algorithm and adjusting it to our needs. Our thanks also go to Marcel Stanitzki for supplying the $e^+e^- \to Z^\star$ sample and to Przemyslaw Majewski for all his help. Last but not least, we thank the other members of the LCD group, in particular Lucie Linssen and Burkhard Schmidt, for useful discussions.

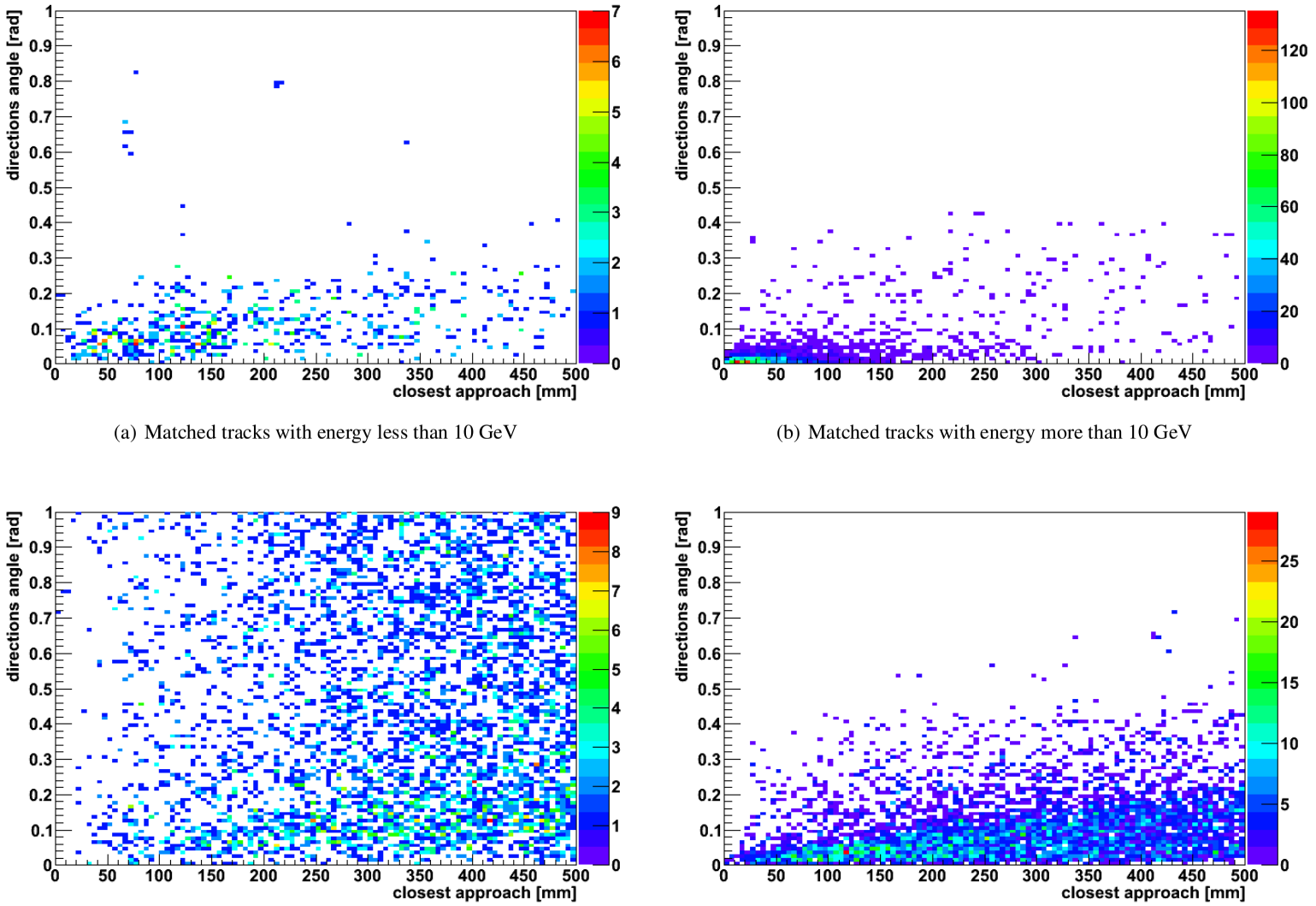

(a) Matched tracks with energy less than 10 GeV

(b) Matched tracks with energy more than 10 GeV

(c) Non-matched tracks with energy less than 10 GeV

(d) Non-matched tracks with energy more than 10 GeV

Figure 9: *Correlation between the opening angle and the distance of closest approach between the extrapolated helix and the yoke track, obtained from the b-jets sample, see Section 1.3.2. Only clusters in the muon system checked to originate from muons are considered; all extrapolated ID-tracks are taken into account. In the upper plots the ID-tracks are truly created by muons, in the lower plots the ID-track originates from any other particle type. The four plots show the distributions for ID-tracks with less than 10 GeV (left) and more than 10 GeV (right).*

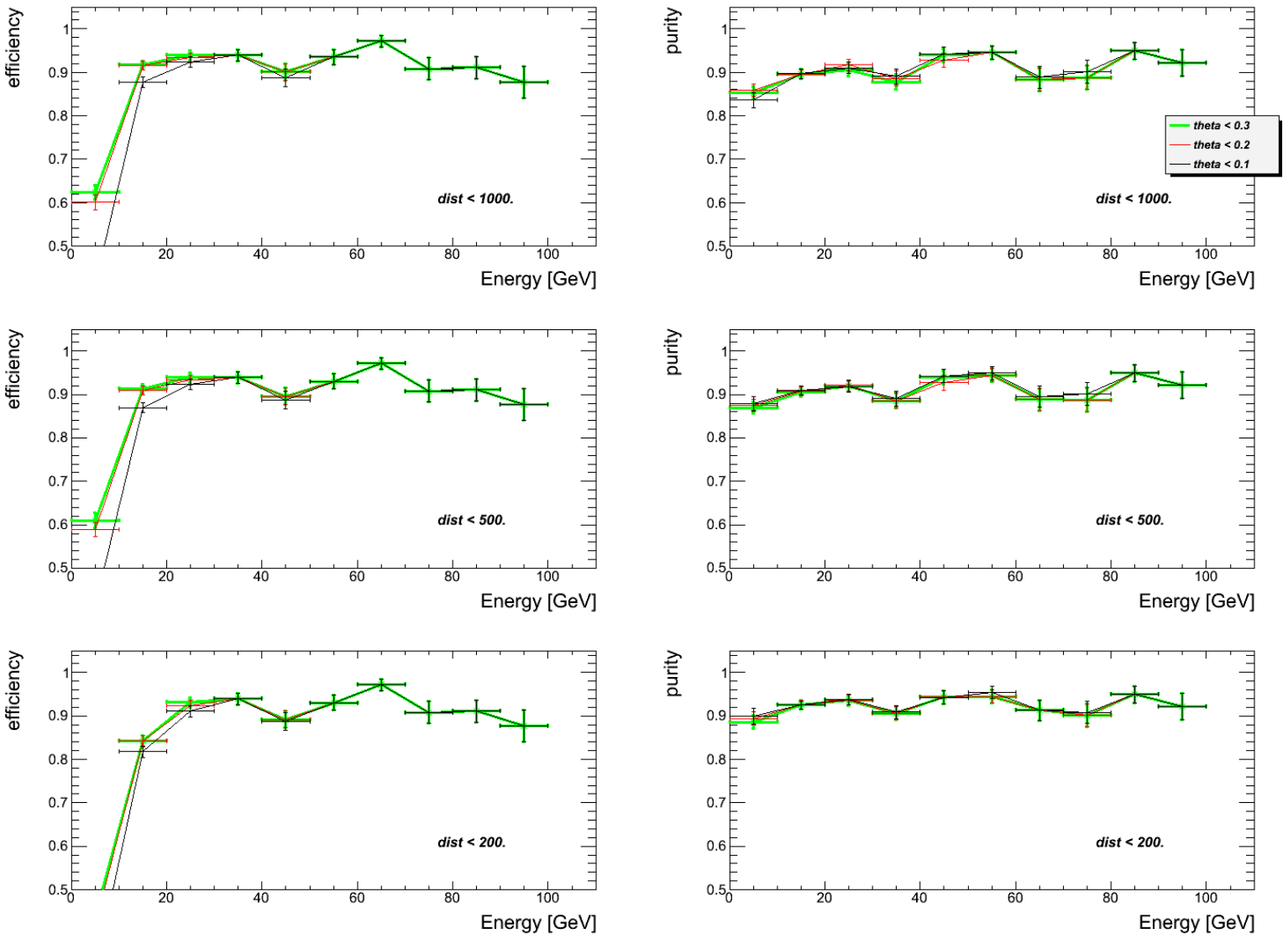

Figure 10: *Efficiency and purity obtained by the muon identification algorithm versus the energy of the muon, extracted from the b-jets sample. Shown is the performance for different values of opening angle between the inner detector track and the yoke track (depicted by different colors) and for the maximum distance between the track helix extrapolation and the most inner yoke hit (see labeling 'dist < XXX').*

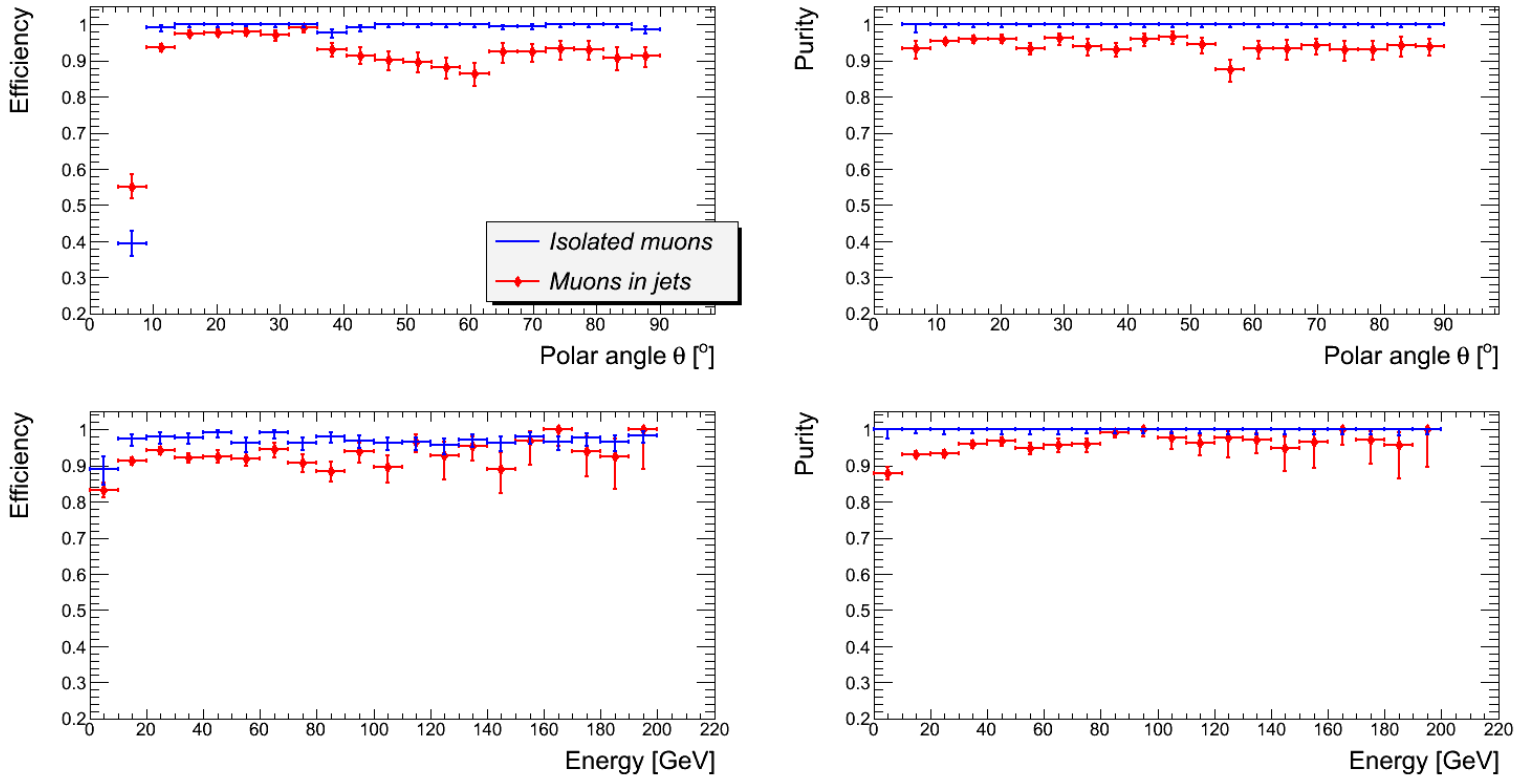

Figure 11: *The identification performance as a function of the energy for isolated muons (from particle gun) and muons in b-jets.*

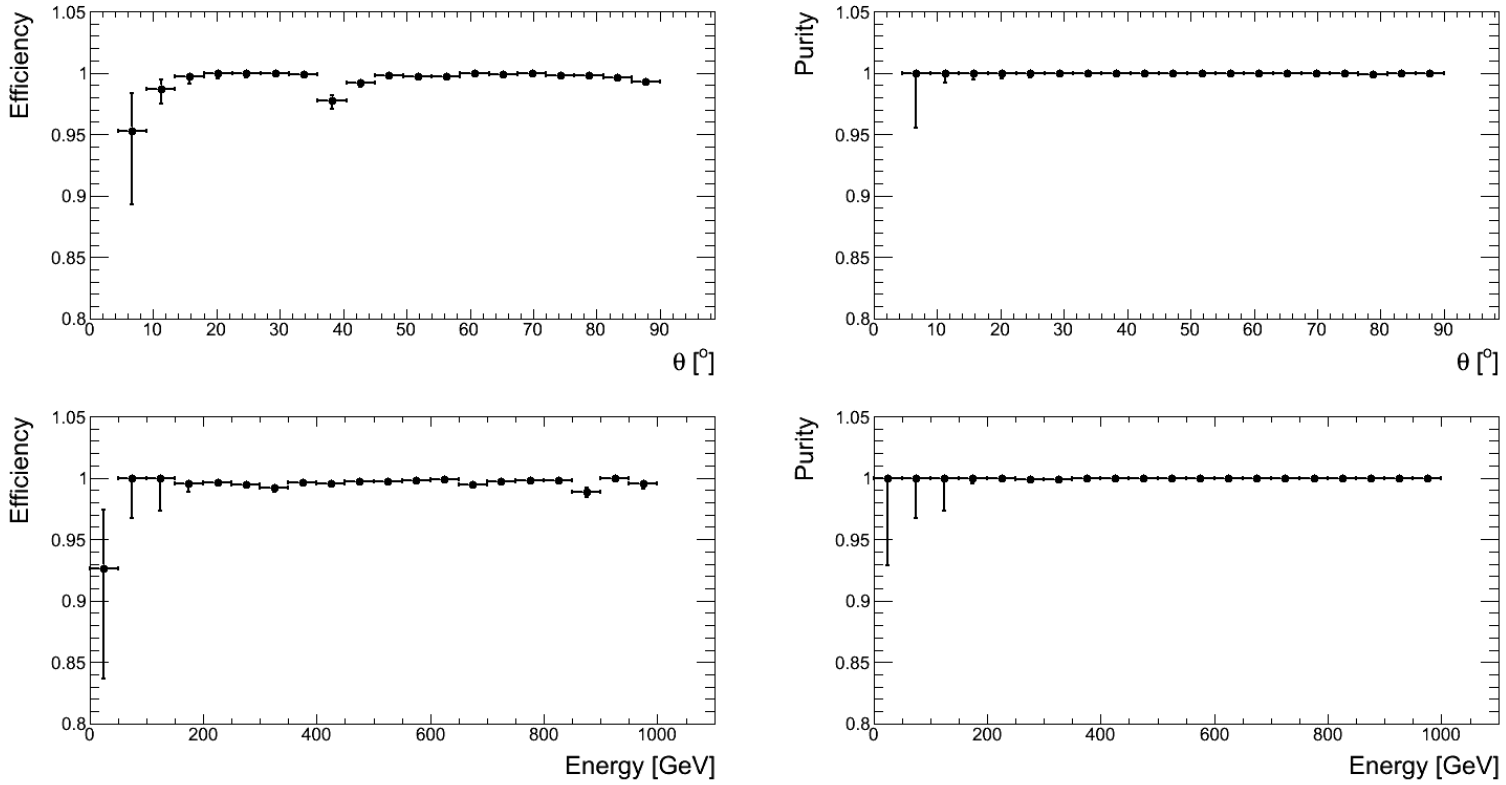

Figure 12: *Efficiency and purity obtained by the muon identification algorithm for high energy muons in the smuon sample.*

References

[1] J. Marshall, Redesign of PandoraPFA, Report at IWLC 2010, October 19, 2010, Geneva.

[2] M. A. Thomson. Particle Flow Calorimetry and the PandoraPFA Algorithm. *Nucl. Instrum. Meth.*, vol. A611 pp. 25–40, 2009. ArXiv:0907.3577.

[3] A. Münnich and A. Sailer. The CLIC ILD CDR Geometry for the CDR Monte Carlo Mass Production. LCD-Note-2011-002, 2011.

[4] E. Van der Kraaij and B. Schmidt. Design of the Muon System for the CLIC Detectors. LCD Note in preparation, 2011.

[5] P. Mora de Freitas and V. H. Detector simulation with mokka/geant4 : Present and future. In *International Workshop on Linear Colliders (LCWS 2002)*. JeJu Island, Korea, 2002.

[6] Marlin website: http://ilcsoft.desy.de/portal/software_packages/marlin/.

[7] J. Nardulli. Particle Identification performance for the CLIC ILD and CLIC SiD detectors. LCD Note in preparation, 2011.

[8] Official CLIC multi-TeV physics benchmark processes for detector performance studies. Website: https://edms.cern.ch/document/1102121/2.

[9] T. Sjöstrand, S. Mrenna, and P. Skands. PYTHIA 6.4 physics and manual. *JHEP*, vol. 05 p. 026, 2006. ArXiv:hep-ph/0603175.

[10] H. Burkhardt, G. A. Blair, and L. Deacon. Muon Backgrounds in CLIC. 1st International Particle Accelerator Conference: IPAC'10, 23-28 May 2010, Kyoto, Japan.

[11] CERN, CLIC Conceptual Design Report, in preparation.

[12] G. Ordonez Sanz. *Muon Identification in the ATLAS Calorimeters*. Ph.D. thesis, Nikhef, 2009.